Ca^{2+} binding sites in calmodulin and troponin C alter interhelical angle movements

Kunihiko Goto[a,*], Akira Toyama[b], Hideo Takeuchi[b], Kazuyoshi Takayama[c], Tsutomu Saito[c], Masatoshi Iwamoto[d], Jay Z. Yeh[a], Toshio Narahashi[a]

[a] *Department of Molecular Pharmacology and Biological Chemistry, Northwestern University Medical School, 303 East Chicago Avenue, Chicago, IL 60611-3008, USA*
[b] *Department of Pharmaceuticals, Graduate School of Pharmaceutical Sciences, Tohoku University, Aobayama, Sendai 980-8578, Japan*
[c] *Shock Wave Research Center, Institute of Fluid Science, Tohoku University, 2-1-1, Katahira, Sendai 980-8577, Japan*
[d] *Department of Applied Physics, Tohoku Gakuin University, 1-13-1, Tagajyo, Miyagi 985-8537, Japan*

Received 13 November 2003; revised 21 January 2004; accepted 26 January 2004

First published online 16 February 2004

Edited by Judit Ovádi

Abstract Molecular dynamics analyses were performed to examine conformational changes in the C-domain of calmodulin and the N-domain of troponin C induced by binding of Ca^{2+} ions. Analyses of conformational changes in calmodulin and troponin C indicated that the shortening of the distance between Ca^{2+} ions and Ca^{2+} binding sites of helices caused widening of the distance between Ca^{2+} binding sites of helices on opposite sides, while the hydrophobic side chains in the center of helices hardly moved due to their steric hindrance. This conformational change acts as the clothespin mechanism.
© 2004 Published by Elsevier B.V. on behalf of the Federation of European Biochemical Societies.

Key words: Molecular dynamics; Conformational change; Calcium binding protein; EF hand; Root mean square difference; Alpha-helix

1. Introduction

Intracellular Ca^{2+} ions serve as a second messenger in response to external stimuli. An increase in the cytoplasmic Ca^{2+} ion concentration leads to Ca^{2+} binding to intracellular regulatory proteins, an event that initiates a wide variety of cellular processes. Calmodulin (CaM) [1] is a ubiquitous, multifunctional protein which can bind to, and regulate, at least 30 different target enzymes and proteins. Troponin C (TnC) [2] plays a crucial role in muscle contraction [3–6]. CaM consists of two similar domains, each containing two Ca^{2+} binding sites. Each Ca^{2+} binding site is made of a so-called EF hand helix-loop-helix motif (hereafter referred to as CI, CII, CIII, and CIV counting from the N-terminus to the C-terminus). CIII and CIV have higher affinity for Ca^{2+} ions than CI and CII [7–12].

TnC also has two globular domains connected by a long central helix. Both domains contain two pairs of Ca^{2+} binding sites, each having an EF hand motif, hereafter referred to as TI, TII, TIII, and TIV counting from the N-terminus to the C-terminus. TIII and TIV have high affinity Ca^{2+}/Mg^{2+} sites, and most likely assume a structural role [13], while TI and TII have lower affinity for Ca^{2+}/Mg^{2+}, and perform the regulatory function by interacting with TnI [13].

Nuclear magnetic resonance (NMR) studies with CaM and TnC in Ca^{2+}-free solutions [14,15] indicate that the Ca^{2+} binding moieties are too far apart to bind Ca^{2+} ions. However, these moieties do bind Ca^{2+} ions as revealed by X-ray crystallographic studies of Ca^{2+}-bound CaM and TnC [14,16]. These results suggest that there are large conformational changes in CaM and TnC to bring the Ca^{2+} binding moieties close enough to bind Ca^{2+} ions. At the same time, CaM and TnC expose their hydrophobic sites to which other proteins can bind [17–19].

Since previous molecular dynamics (MD) studies had focused either on the Ca^{2+}-free structure by using NMR or on the Ca^{2+}-bound structures by using X-ray crystallography [20–25], the way in which Ca^{2+} binding to CaM and TnC induces conformational changes has not been examined. Here, we modified the Ca^{2+} binding moieties of the NMR-based structure without altering its backbone such that they can bind to Ca^{2+} ions. From this initially modified Ca^{2+}-bound CaM and TnC, MD simulation was initiated. We observed conformational changes leading to the final structure deduced from NMR and X-ray crystallographic studies [20–26] with Ca^{2+} bound structures. The Ca^{2+} binding induced conformational changes in the backbones of CaM and TnC opening up the hydrophobic sites to which other regulatory proteins could bind [17–19].

2. Materials and methods

2.1. MD systems

The initial coordinates of CaM were taken from the Protein Data Bank, PDB code 1CFC, model 14 [27]. For TnC, the initial coordinates were taken from PDB code 1TNP, model 17 [14]. Both structures were based on NMR studies. To reduce the size of the analysis system, we used the C-terminus (residues 80–148) of CaM, Ca^{2+} binding proteins of *Xenopus laevis* [27], and the N-terminus (residues 1–90) of TnC [14].

All energy minimizations and MD analyses were performed using InsightII/Discover (Accelrys Japan, Tokyo, Japan). Ca^{2+} ions were placed at two Ca^{2+} binding pockets of CaM or TnC. The binding pockets were created by moving the Ca^{2+} binding moieties towards the Ca^{2+} ions while keeping the main chain fixed. Thus, this system was minimized.

*Corresponding author. Fax: (1)-312-503 1700.
E-mail address: kunihikogoto@aol.com (K. Goto).

Abbreviations: CaM, calmodulin; TnC, troponin C; RMSD, root mean square difference

0014-5793/04/$30.00 © 2004 Published by Elsevier B.V. on behalf of the Federation of European Biochemical Societies.
doi:10.1016/S0014-5793(04)00114-0

Depending on the number and locations of Ca^{2+} ions in the initial model, four configurations of CaM and of TnC were designated and their nomenclatures are defined in Fig. 1A. CIII and CIV of CaM and TI and TII of TnC made up the Ca^{2+} binding pockets. In the X-ray structure of the Ca^{2+}-bound form [16], each site of CIII, CIV, TI and TII was occupied by a Ca^{2+} ion. Initial structures of PCa0, PCa1, PCa2, and PCa3 were identical. No Ca^{2+} ion was included for PCa0. For PCa1, one Ca^{2+} ion was included at site CIII. For PCa2, one Ca^{2+} ion occupied site CIV. In PCa3, sites CIII and CIV were each occupied by one Ca^{2+} ion.

In TnC (Fig. 1A), initial structures of PTn0, PTn1, PTn2, PTn3, and PTn4 were identical. For PTn0 no Ca^{2+} ion was included. For PTn1, one Ca^{2+} ion was included at site TI. For PTn2, one Ca^{2+} ion occupied site TII. In PTn3, sites TI and TII were each occupied by one Ca^{2+} ion. Four MD analyses of the C-terminal domain of CaM and the N-terminal domain of TnC were performed.

The initial structures were immersed in a box with 44, 36, and 30 Å in the x, y, and z directions with water molecules (Fig. 1B,C). Finally, potassium ions were included to bring the system to neutrality. The resulting size of the total system was 3421–3423 atoms in CaM: 1032 protein atoms, 0–2 calcium ions, and 8–12 potassium ions, and 2379 water molecules (Fig. 1B). In TnC, the size was 4529–4533 atoms: 1347 protein atoms, 0–2 calcium ions, and 12–16 potassium ions, and 3168 water molecules (Fig. 1C).

Initially, the system was minimized for 300 conjugate gradient steps, while keeping the protein, Ca^{2+} ions, and potassium ions fixed. After a 300 ps equilibration period, the system was subjected to another 300 conjugate gradient minimization steps when all fixed atoms were set free to move. The full system was then equilibrated under the same condition as above for 1 ns, saving coordinates every 0.5 ps. The particle mesh Ewald method was used for the computation of electrostatics without cutoff [28]. All analyses were performed using CFF force field [29] and the MD program Discover, with periodic boundary conditions at a constant temperature of 298 K and constant pressure of 1 atm (NpT ensemble). Langevin dynamics and Langevin piston methods were used to keep temperature and pressure constant.

2.2. Interhelical angle calculation

Interhelical angles were calculated using a program written by I. Sato of Miyagi Prefecture Cancer Center, Japan. The starting and end points of helices used for the calculation were as follows: residues 82–92 for E, residues 102–111 for F, residues 118–128 for G, and residues 138–146 for H in CaM (Fig. 4A); residues 16–29 for A, residues 39–47 for B, residues 55–64 for C, and residues 75–86 for D in TnC (Fig. 4B).

3. Results and discussion

3.1. Root mean square difference (RMSD) in CaM and TnC

We examined how Ca^{2+} ions induced conformational changes in the Ca^{2+} binding proteins CaM and TnC using a MD approach. The initial structure of Ca^{2+} binding and its nomenclature of CaM are shown in Fig. 1. In PCa0 of CaM, 1 ns RMSD of the main chain (Fig. 2A) showed that the deviation size in PCa0 without Ca^{2+} binding was around 3 Å, a value approximately compatible with the results of previous MD simulations [22,25]. Ca^{2+} binding to CaM increased RMSD as the deviation size in PCa2 was higher, and those in PCa1 and PCa3 were the highest, reaching a similar amplitude of 5 Å (Fig. 2A,B). These findings indicated that Ca^{2+} binding to CaM induced a large conformational change. During the critical first 200 ps (Fig. 2A,B), RMSD of PCa2 and PCa3 increased rapidly for the first 20 ps, followed by a slower phase in the next 180 ps. Despite a similarity of increase in amplitude of RMSD, PCa1 had a much slower increase in RMSD than PCa3 in the first 200 ps (Fig. 2A,B).

The initial structure of Ca^{2+} binding and its nomenclature of TnC are illustrated in Fig. 1A,C. In TnC, RMSD was lowest in PTn0, and increased in the following ascending order: PTn2 < PTn1 < PTn3 (Fig. 2C,D). These findings showed

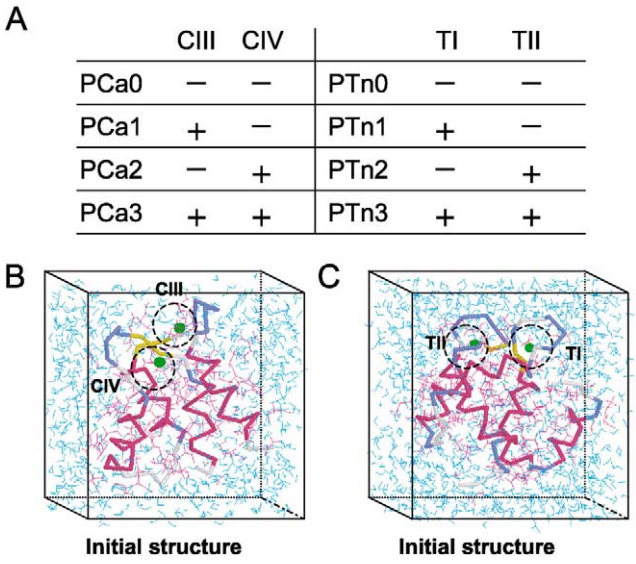

Fig. 1. A: Nomenclature of four configurations of CaM and TnC and their corresponding Ca^{2+} binding states. B: Initial structure of CaM. C: Initial structure of TnC. The calcium density is represented by spacefill 200 model. The ribbon model red spiral molecules, α-helix; yellow molecules, β-sheet; light blue, loop; gray, random coil. The diagram was prepared with the Rasmol program.

that Ca^{2+} binding to TnC caused a large conformational change as seen in the case of CaM. However, Ca^{2+} binding induced a larger conformational change with TnC than with CaM. For example, RMSD with PTn3 reached 6.5 Å whereas that with PCa3 reaches near 5 Å. As the RMSD change was essentially complete within the first 200 ps, we placed our emphasis on the analysis of conformational changes within the first 200 ps.

3.2. Changes of interhelical angles in CaM and TnC

Interhelical angle changes in PCa3 with two Ca^{2+} ions were the largest (Fig. 3A1), those in PCa1 and PCa2 with one Ca^{2+} ion were smaller (Fig. 3A2), and those in PCa0 were the smallest (Fig. 3A1), as seen with changes in terms of RMSD.

In PCa0, PCa1, and PCa2, the opening of hydrophobic subsites to which CaM binding proteins can bind [17] did not occur. These findings would be explained by the finding that, in PCa1, the binding of Y99.o, E104.oe2, and E104.oe1 with Ca^{2+} ions was lost from the 18 ps structure, and that, in PCa2, the binding of Q135.o with Ca^{2+} was lost from 26 ps. The interhelical G/H and E/F angles of the 120–140 ps structure were very similar to those of the Ca^{2+} binding form detected by NMR [26] and X-ray crystallography [15] (Fig. 4C). The overall backbone RMSD between this MD and NMR results was 0.8 Å, while that between the MD and X-ray crystal structures was 1.1 Å. Nevertheless, a 7° change in the orientation of helix E between MD and NMR structures and a 10° change between the MD and X-ray crystal results were visible, while a smaller change for helix H was observed (Fig. 4C). In this analysis, two Ca^{2+} bindings were maintained throughout, and the opening of hydrophobic subsites occurred (Fig. 4A,D).

Changes of interhelical angles in the TnC structures, PTn0, PTn1, PTn2, and PTn3 (Fig. 3A1,A2) were similar to those in PCa0, PCa1, PCa2, and PCa3 of CaM, respectively (Fig. 3B1,B2). The interhelical C/D and A/B angles of around

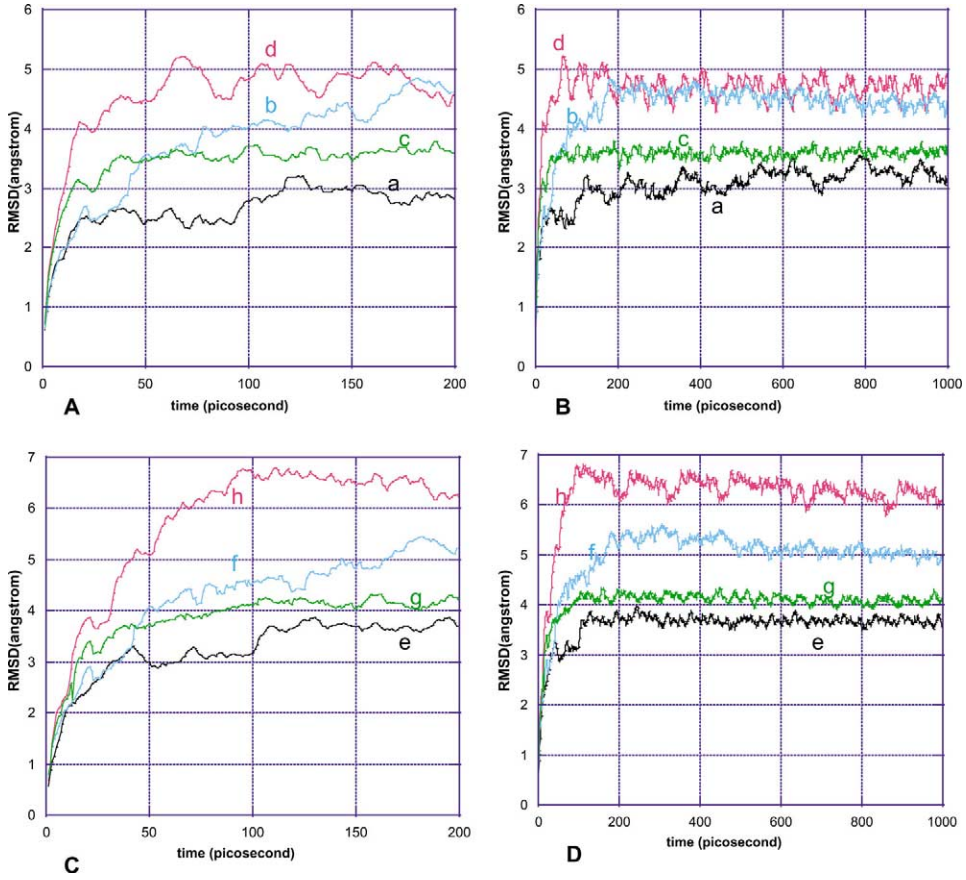

Fig. 2. RMSD in CaM and TnC. A,B: CaM. Black line a, PCa0; cyan line b, PCa1; green line c, PCa2; red line d, PCa3. C,D: TnC. Black line e, PTn0; cyan line f, PTn1; green line g, PTn2; red line h, PTn3. Note that large conformational changes occurred within 200 ps.

150 ps structure in PTn3 were very similar to those of the Ca^{2+}-bound form detected by X-ray crystallography [14,30,31]. In PTn3, the opening of hydrophobic subsites was observed (Fig. 4B) and two Ca^{2+} bindings were maintained throughout in the same manner as in PCa3 of CaM (Figs. 3B1 and 5D–F).

3.3. Conformational changes in PCa3 and PTn3

In PCa3, the CIII and CIV sites were each occupied by one Ca^{2+} ion. At the CIV Ca^{2+} binding site of CaM, the Ca^{2+} attracted oε1 and oε2 of D133 of the non-helical regions between helices G and H and the same Ca^{2+} ion also attracted oε1 and oε2 of E140 of the H helix (from 0 ps to 20 ps). These Ca^{2+} binding forces caused D133.cα to become near E140.cα (Fig. 4A) and caused the N-terminus D118.cα, the opposite side of the G helix, to move far from the C-terminus, T146.cα, the opposite side of the H helix, because large hydrophobic subsites, I125 in helix G and F141 in helix H, hardly moved due to their steric hindrance (Fig. 4A). In the CIII Ca^{2+} binding site, the Ca^{2+} attracted oε1 and oε2 of E104 of helix F and the same Ca^{2+} ion attracted oδ1 and oδ2 of D95 of the non-helical loop between helices E and F due to Ca^{2+} binding force, resulting in E104.cα becoming near D95.cα (Fig. 4A). The N-terminus, E82.cα, the opposite side of helix E, moved far from the C-terminus, N111.cα, the opposite side of helix F, because large hydrophobic subsites, F89 of helix E and V108 of helix F, hardly moved due to their steric hindrance (Figs. 4A and 5A). These findings common to CIV and CIII suggested that binding forces among two Ca^{2+} ions and Ca^{2+} binding sites of helices E, F, G, and H shortened the distance between Ca^{2+} and Ca^{2+} binding sites of helices E and F and between Ca^{2+} and Ca^{2+} binding sites of helices G and H, resulting in a widening of the distance between the opposite sides of Ca^{2+} binding sites of helices as the large hydrophobic side chains in the center of helices hardly moved due to their steric hindrance (clothespin mechanisms) (Fig. 5A).

The critical role of large hydrophobic subsites in CaM has been supported by the findings that the substitution of alanine for one or more phenylalanine induced functional defects [32] and that F92A disordered the conformational changes [33]. Thus, these findings would be explained by the mechanisms that, because the center hydrophobic subsites with alanine are small as compared to phenylalanine, the shortening of Ca^{2+} binding sites fails to induce widening on the opposite sides of Ca^{2+} binding sites. The clothespin mechanism is similar to the prediction from the static structures proposed by Richardson and Richardson [34]. Contacts of lap-joint helices which they called α-helix-loop-α-helix structure in Ca^{2+} binding proteins and DNA binding proteins consist of large hydrophobic side chains. They suggested conformational change using the closest backbone (of large hydrophobic side chains) contact as a pivot. However, they did not examine how Ca^{2+} binding proteins induced conformational changes, because they did not use MD approaches.

In the TII Ca^{2+} binding site of TnC in PTn3, the Ca^{2+} ion attracted oδ1 and oδ2 of D68 in the non-helical regions be-

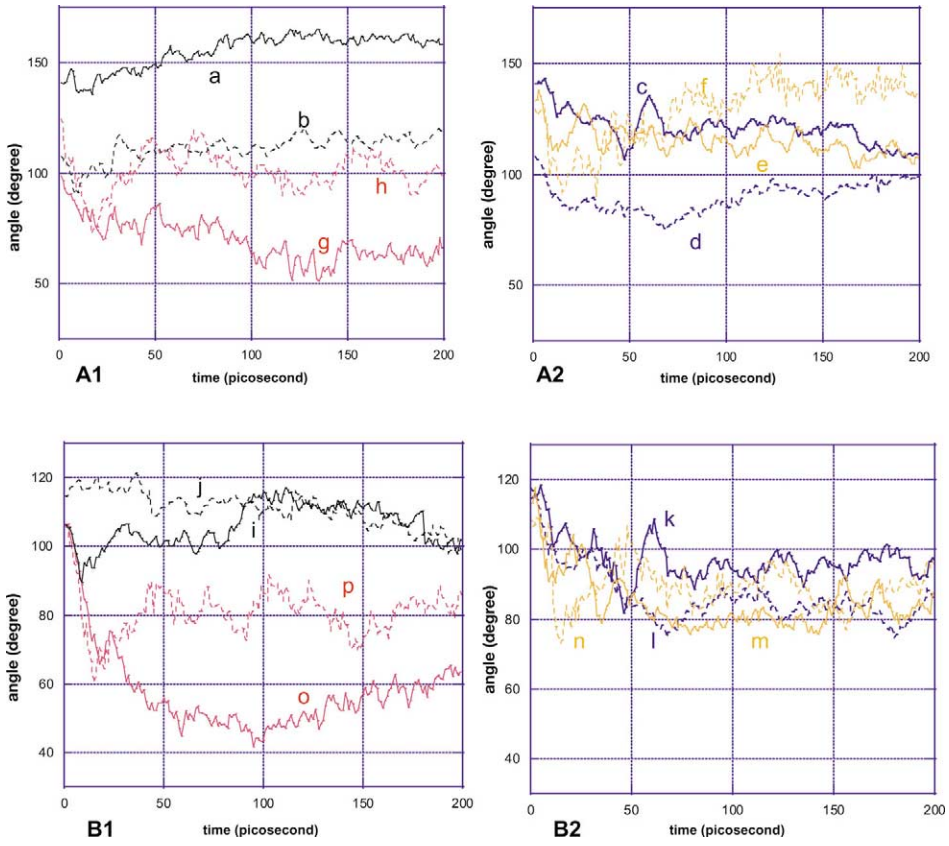

Fig. 3. A1: Interhelical angle changes in PCa0 and PCa3 configurations of CaM. Black line a, the E/F angle between E/F helices in PCa0; black dotted line b, the G/H angle in PCa0; red line g, the E/F angle change in PCa3; red dotted line h, the G/H angle change in PCa3. A2: Interhelical angle changes in PCa1 and PCa2 configurations of CaM. Light blue line c, the E/F angle changes in PCa1; light blue dotted line d, the G/H angle changes in PCa1; yellow line e, the E/F angle changes in PCa2; yellow dotted line f, the G/H angle changes in PCa2. B1: Interhelical angle changes in PTn0 and PTn3 configurations of TnC. Black line i, the A/B angle between A/B helices in PTn0; black dotted line j, the C/D angle in PTn0; red line o, the A/B angle changes in PTn3; red dotted line p, the C/D angle changes in PTn3. B2: Interhelical angle changes in PTn1 and PTn2 configurations of TnC. Light blue line k, the A/B angle changes in PTn1; light blue dotted line l, the C/D angle changes in PTn1; yellow line m, the A/B angle changes in PTn2; yellow dotted line n, the C/D angle changes in PTn2.

tween helices C and D and at the same time it pulled oε1 and oε2 of E77 of helix D due to the Ca^{2+} binding force, resulting in D68.cα becoming close to E77.cα (Fig. 4B). The N-terminus, K55.cα, the opposite side of helix C, became far away from the C-terminus, M86.cα, the opposite side of helix D, because large hydrophobic subsites, V65 in the non-helical regions between C and D and V80 in helix D, hardly moved due to their steric hindrance (Fig. 4B). In the TI Ca^{2+} binding site, the Ca^{2+} ion attracted oε1 and oε2 of E41 of helix B and the same Ca^{2+} ion pulled oδ1 and oδ2 of D32 of the non-helical loop between A and B due to the Ca^{2+} binding force, resulting in E41.cα becoming close to D32.cα (Fig. 4B). The N-terminus, E16.cα, the opposite side of helix A, became far away from the C-terminus, R47.cα, the opposite side to helix B, because large hydrophobic subsites, F29 in helix A and V45 in helix B, hardly moved due to their steric hindrance (Figs. 4B and 5B). These findings common to TI and TII suggested that binding forces between two Ca^{2+} ions and Ca^{2+} binding sites of helices A, B, C, and D shortened the distance of helices A and B and at the same

Fig. 4. A: Ca^{2+} binding sites and helices in the CaM 130 ps structure. Stereographs at 130 ps in CaM viewed from the upper part of the Ca^{2+} binding sites of helices which opened. Backbone model, main chain (red, α-helix; blue, random coil; white, loop); green spacefill 200 model, Ca^{2+}; magenta ball and stick model, Ca^{2+} binding oxygen atoms; wire frame model, hydrophobic side chain. B: TnC 150 ps structure. The N helix was removed. Note that the β-sheet between TnI and TnII loops was lost, and that the α-helix of B helix was broken (compare with Fig. 1C). C: Stereographs of the MD structure, shown in red, the NMR structure in green (1J7P), and the X-ray structure (1CLL) in blue. For the C-terminal domain, residues 102–128 (helices F and G) are superimposed, showing much smaller orientation differences of 10 and 7° for helices E and H, respectively. D: The parallel α-helix slidings in PCa1. Left side, Ca^{2+} binding sites viewed from the upper part of Ca^{2+} binding sites; middle, maximal interhelical angle image; right side, 90° rotation in *y*-axis of the middle figure. E: The parallel α sliding in PCa2. F: The parallel α slidings in mutant$^{F92/F141G}$. Note in A that the hydrophobic subsites open, that β-sheet which had been built between CIII and CIV loops was cut, and that α-helix of G helix was broken (compare with Fig. 1B). Note in C–E that opening of hydrophobic sites in PCa1, PCa2, and mutant$^{F92/F141G}$ did not occur and that results of parallel α-helix sliding caused interhelical angles to wrench largely, and induced the exposure of the embedded surfaces of helices F and G.

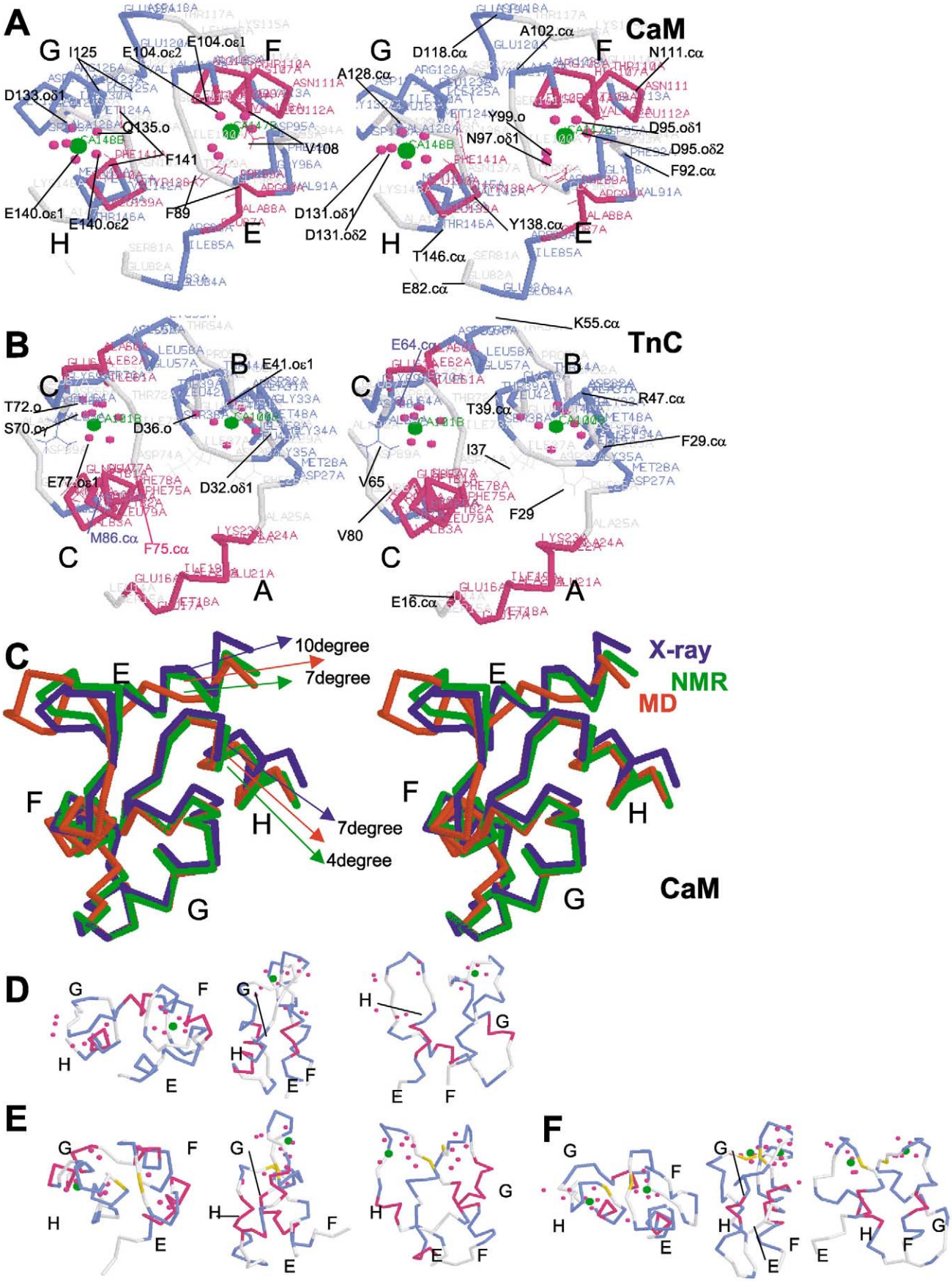
A
G
I125
E104.oε2
E104.oε1
F
D133.oδ1
Q135.o
V108
F141
E140.oε1
E140.oε2
F89
H
E
CaM
D118.cα
A102.cα
N111.cα
A128.cα
Y99.o
D95.oδ1
N97.oδ1
D95.oδ2
F92.cα
D131.oδ1
D131.oδ2
Y138.cα
T146.cα
E82.cα
B
C
B
E41.oε1
T72.o
S70.oγ
D36.o
E77.oε1
D32.oδ1
M86.cα
F75.cα
C
A
TnC
K55.cα
E64.cα
R47.cα
T39.cα
F29.cα
I37
V65
F29
V80
E16.cα
C
10degree
7degree
E
F
H
7degree
4degree
G
X-ray
NMR
MD
CaM
D
E
F

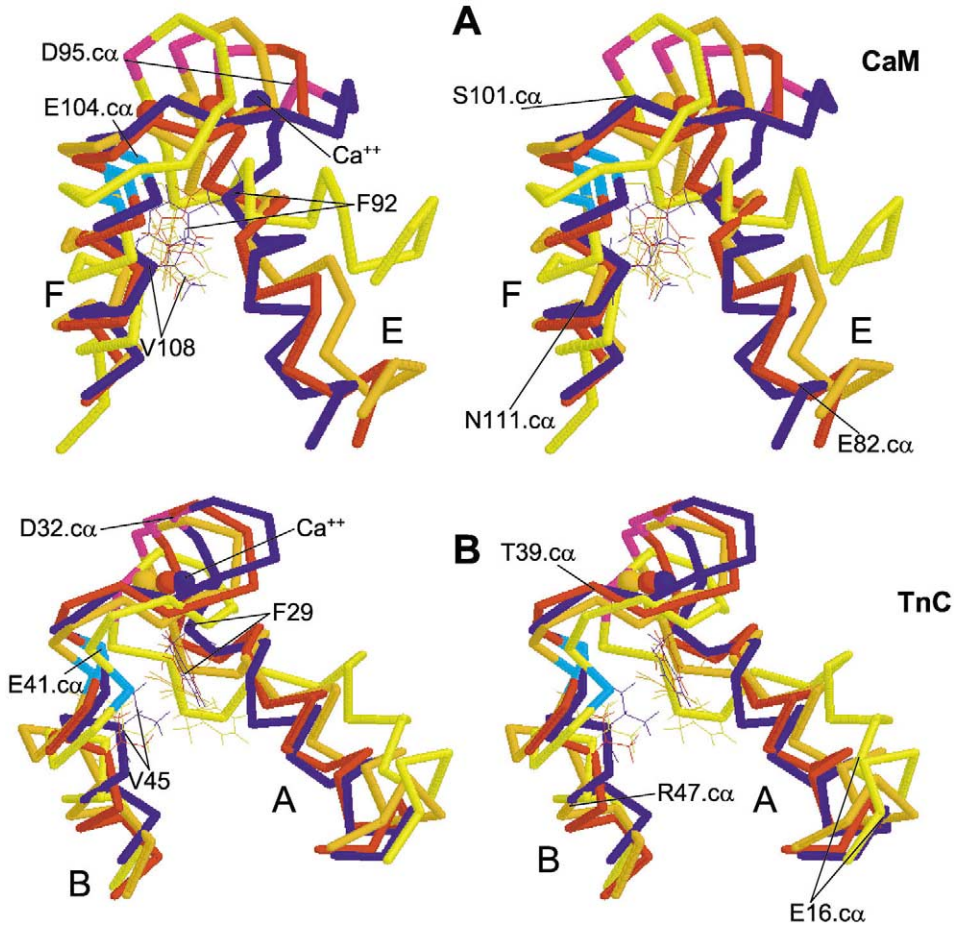

Fig. 5. A: Stereo view of conformational changes in the CIII region of CaM. Backbone model blue line, initial structure; red line, 17 ps structure; orange line, 50 ps structure; yellow, 130 ps structure. Ball model, Ca^{2+} ion; backbone model magenta line, D95.cα; backbone cyan line, E104.cα; wire frame line, F92 and V108. B: Stereo view of conformational changes in the TI region of TnC. Backbone model blue line, initial structure; red line, 25 ps structure; orange line, 80 ps structure; yellow, 150 ps structure. Ball model, Ca^{2+} ion; backbone model magenta line, D32.cα; backbone model cyan line, E41.cα; wire frame line, F29 and V45.

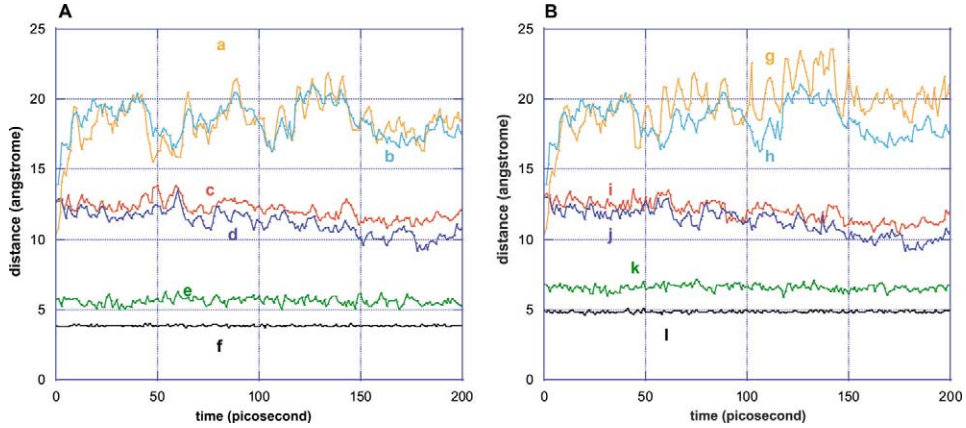

Fig. 6. A: Changes in interhelical distance, Ca^{2+} binding site region, and hydrophobic subsites in CaM. Orange line a, changes in the distance between the N-terminus of helix E and the C-terminus of helix F; light blue line b, changes of distance between the N-terminus of helix G and the C-terminus of helix H; red line c, changes in the distance between E104.cα and D95.cα; blue line d, changes in the distance between E140.cα and D131.cα; green line e, changes in the distance between V108.cα and F92.cα; black line f, changes in the distance between I125.cα and F141.cα. B: Changes in the interhelical distance, Ca^{2+} binding site region, and hydrophobic subsites in TnC. Orange line g, changes in the distance between the N-terminus of helix A and the C-terminus of helix B; light blue line h, changes in the distance between the N-terminus of helix C and the C-terminus of helix D; red line i, changes in the distance between D32.cα and E41.cα; blue line j, changes in the distance between S70.cα and E77.cα; green line k, changes in the distance between F29.cα and V45.cα; black line l, changes in the distance between V65.cα and V80.cα.

time widened the opposite sides of Ca^{2+} binding site of helices because the large subsites would work as a pivot. Namely the distance between Ca^{2+} and Ca^{2+} binding sites of helices C and D is widened. Mechanically, this works like a clothespin mechanism.

In order to estimate this suggestive clothespin mechanism, first in CaM, we calculated the distance between Ca^{2+} binding sites, that between hydrophobic side chains, and that between the opposite sites to Ca^{2+} binding sites (the tail of clothespin to become opened) (Fig. 6A). We found that the distance between Ca^{2+} binding sites became short, and that between the opposite sites to Ca^{2+} binding sites became long, while the distance between the hydrophobic side chains hardly changed (Fig. 6A). These findings strongly suggested that the clothespin mechanism worked in the conformational changes in CaM (Fig. 6A). Thus, the energy provided by Ca^{2+} binding is the driving force to shorten the distance between the Ca^{2+} binding sites just as the mechanical force is to squeeze the head of the clothespin together. In the CIV Ca^{2+} binding site, the shortening of the distance between D131.cα and E140.cα by Ca^{2+} binding is the driving force of opening the hydrophobic subsites. Experiments using the backbone dynamics of E140Q would support the clothespin mechanism [35]. We observed a similar phenomenon in TnC (Fig. 6B).

The phenomenon that steric hindrance of large hydrophobic side chains plays a role in conformational changes is commonly observed, and suggests that this steric hindrance should be included in models of the interaction of macromolecules, e.g. in the 'rotation model' [36–41].

Furthermore, to estimate the clothespin mechanism, we prepared mutant$^{V108G/F92G}$, mutant$^{I125G/F141G}$, mutant$^{F92G/F141G}$ and mutant$^{V108G/F92G/I125G/F141G}$. One nanosecond MD analysis of these mutants showed that interhelical angles in all mutants decreased by 35–45° (not shown) in almost the same size as observed in PCa3 and that parallel interhelical slidings occurred similar to the results in PCa1 and PCa2 (compare Fig. 4F with D,E). The opening of hydrophobic subsites was not observed and rather mutants became compacted (compare Fig. 4F and A).

Acknowledgements: We deeply thank Haruo Yoshikoshi of Tohoku-kensetsukyokai for encouragement, Ikuro Sato for statistics, Tadahiro Ohmura, Masayuki Mori of Accelrys Japan, and Yamagishi of SGI Japan for simulation techniques.

References

[1] Kakiuchi, S. and Yamazaki, R. (1970) Biochem. Biophys. Res. Commun. 41, 1104–1110.
[2] Ebashi, S. (1960) J. Biochem. 48, 150–158.
[3] Leavis, P.C. and Gergeley, J. (1984) CRC Crit. Rev. Biochem. 16, 235–305.
[4] Zot, A.S. and Potter, J.D. (1987) Annu. Rev. Biophys. Biophys. Chem. 16, 535–559.
[5] Ohtsuki, I., Maruyama, K. and Ebashi, S. (1986) Adv. Protein Chem. 38, 1–67.
[6] Farah, C.S. and Reinach, F.C. (1995) FASEB J. 9, 755–767.
[7] Ikura, M. et al. (1983) Biochemistry 22, 2573–2579.
[8] Andersson, A., Forsen, S., Thulin, E. and Vogel, H.J. (1983) Biochemistry 22, 2309–2313.
[9] Dalgarno, D.C. et al. (1984) Eur. J. Biochem. 138, 281–289.
[10] Minowa, O. and Yagi, K. (1984) J. Biochem. 96, 1175–1182.
[11] Klee, C.B. (1988) In: Calmodulin (Cohen, P. and Klee, C.B., Eds.), pp. 35–56, Elsevier, New York.
[12] Linse, S., Hjalmersson, A. and Forsen, S. (1991) J. Biol. Chem. 266, 8050–8054.
[13] Grabarek, Z., Tao, T. and Gergely, J. (1992) J. Muscle Res. Cell Motil. 13, 383–393.
[14] Gagne, S.M., Tsuda, S., Li, M.X., Smillie, L.B. and Sykes, B.D. (1995) Nat. Struct. Biol. 2, 784–789.
[15] Zhang, M., Tanaka, T. and Ikura, M. (1995) Nat. Struct. Biol. 2, 758–767.
[16] Chattopadhyaya, R., Weador, W.E., Means, A.R. and Quiocho, F.A. (1995) J. Mol. Biol. 228, 1177–1195.
[17] Meador, W.E., Means, A.R. and Quiocho, F.A. (1992) Science 257, 1251–1255.
[18] Li, Y., Love, M.L., Putkey, J.A. and Cohen, C. (2000) Proc. Natl. Acad. Sci. USA 97, 5140–5145.
[19] Vassylyev, D.G., Takeda, S., Wakatsuki, S., Maeda, K. and Maeda, Y. (1998) Proc. Natl. Acad. Sci. USA 95, 4847–4852.
[20] Van Der Spoel, D., De Groot, B.L., Hayward, S., Berendsen, H.J.C. and Vogel, H.J. (1996) Protein Sci. 5, 2044–2053.
[21] Wriggers, W., Mehler, E., Pitici, F., Weinstein, H. and Schulten, K. (1998) Biophys. J. 74, 1622–1639.
[22] Vigil, D., Gallagher, S.C., Trewhella, J. and Garcia, A.E. (2001) Biophys. J. 80, 2082–2092.
[23] Yamaotsu, N., Suga, M. and Hirono, S. (2001) Biopolymers 58, 410–421.
[24] Yang, C., Jas, G.S. and Kuczera, K. (2001) J. Biomol. Struct. 19, 247–271.
[25] Komeiji, Y., Ueno, Y. and Uebayasi, M. (2002) FEBS Lett. 521, 133–139.
[26] Chou, J.J., Li, S., Klee, C.B. and Bax, A. (2001) Nat. Struct. Biol. 8, 990–997.
[27] Kuboniwa, H., Tjandra, N., Grezesiek, S., Ren, H., Klee, C.B. and Bax, A. (1995) Nat. Struct. Biol. 2, 768–776.
[28] Darden, T., York, D. and Pedersen, L. (1993) J. Chem. Phys. 98, 10089–10092.
[29] Hwang, M.J., Stockfisch, T.P. and Hagler, A.T. (1994) J. Am. Chem. Soc. 116, 2515–2518.
[30] Houdusse, A., Love, M.L., Dominguez, R., Grabarek, Z. and Cohen, C. (1997) Structure 5, 1695–1711.
[31] Strynadka, N.C., Cherney, M., Sielecki, A., Li, M.X., Smillies, L.B. and James, M.N.G. (1997) J. Mol. Biol. 273, 238–255.
[32] Ohya, Y. and Botstein, D. (1994) Science 263, 963–966.
[33] Meyer, D.F., Mabuchi, Y. and Grabarek, Z. (1996) J. Biol. Chem. 271, 11284–11290.
[34] Richardson, J.S. and Richardson, D.C. (1988) Proteins 4, 229–239.
[35] Evanas, J., Forsen, S., Malmendal, A. and Akke, M. (1999) J. Mol. Biol. 289, 603–617.
[36] Goto, K. (1983) Tohoku J. Exp. Med. 139, 159–164.
[37] Goto, K. (1994) J. Theor. Biol. 170, 267–272.
[38] Goto, K. (1995) Biochem. Biophys. Res. Commun. 206, 497–501.
[39] Goto, K. and Iwamoto, M. (1997) Tohoku J. Exp. Med. 182, 15–33.
[40] Goto, K. (1998) Prog. Anesth. Mech. 5, 1–22.
[41] Goto, K. et al. (2004) J. Mem. Biol., submitted.